Influence of the Elastic Field of Quantum Dots on the Electronic Band Structure of III-Nitride Wire Semiconductors

Nguyen Van Tuyen [1,2,*], A.L. Kolesnikova [2] (iD), A.E. Romanov [1] (iD)

[1] ITMO University, 49 Kronverksky pr., St. Petersburg, 197101, Russia
[2] Sao Do University, No 24, Thai Hoc 2, Sao Do Ward, Chi Linh City, Hai Duong, Vietnam
[3] Institute for Problems in Mechanical Engineering of the Russian Academy of Sciences, 61 Bolshoj pr., V.O., St. Petersburg, 199178, Russia

Article history	Abstract
	In this work, we investigate the effect of the strains induced by axially symmetric quantum dots of cylindrical, hemispherical and conical shapes in a III-nitride semiconductor nanowire on the band structure of the nanowire material. To study the elastic properties of quantum dots, a model of an elastic inclusion with eigenstrain has been used. To consider the influence of the free surface of the wire on the elastic fields of quantum dots, the corresponding boundary value problems have been solved analytically. The $\mathbf{k} \cdot \mathbf{p}$ perturbation method has been applied to analyze the strain induced effect on the energy band structure of the material. The results obtained demonstrate that the band gap width clearly depends on the shape of the embedded quantum dot. The effect of quantum dot strains on the electropolarization of the material possessing ferroelectric properties, was investigated. It was shown that the largest jump in electric charge density is achieved near the apex of the conical inclusion.

1. INTRODUCTION

The III-nitride materials (AlN, GaN, InN and their solid solutions) have a unique combination of physical properties that ensure their demand in modern microelectronics and optoelectronics. Among these properties are wide band gaps, high saturation drift velocity, high breakdown voltage, high thermal conductivity, high thermal and chemical stability, etc. [1]. Due to these characteristics, nitrides are currently considered the most promising material for fabricating robust high-frequency transistor structures capable of operating at high temperatures and under harsh operating conditions. Additionally, in ternary semiconductors, such as $In_xGa_{1-x}N$, $Al_yGa_{1-y}N$, etc., the band gap width can be changed from the visible to the deep ultraviolet region by varying the ratio of their components. This allows III-nitride materials to be used in the fabrication of light-emitting diodes, laser diodes, optical sensors that operate in a wide range of the electromagnetic spectrum [2–6]. The distinguishing properties of III-nitride semiconductors include their large spontaneous polarization and large piezoelectric coefficients [7–9]. Strain-induced piezoelectric polarization charges lead to electrostatic fields of a magnitude (MV/cm) that cannot be neglected in nitride semiconductors.

In general, strain strongly affects the electronic properties of semiconductors; both valence and conduction bands can be changed due to strain [10–16]. The elastic properties of quantum dots in the material matrix have garnered significant attention in recent studies due to their important role in materials science and technology [17–20]. The presence of quantum dots (QDs) in semiconductors has a strong influence on the electronic band structure through the strain generated by QDs in the surrounding material matrix. In terms of continuum mechanics, QDs are considered to be elastic inclusions with an eigenstrain corresponding to the mismatch coefficient between the lattice constant of the dots and the surrounding material matrix [21].

For inclusions of different shapes, the computation of the elastic field requires different numerical techniques. Among these, the elastic inclusion model proposed by Es-

---

* Corresponding author: Nguyen Van Tuyen, e-mail: nguyenvantuyendhsd@gmail.com

helby (see Refs. [22,23]) is a powerful tool that has been widely used to address a variety of elastic field problems involving inhomogeneities and elastic inclusions in solids. Furthermore, for inclusions with axial symmetry, finding analytical solutions can be simplified if we model the inclusion as infinitesimally thin disks distributed along the axis of symmetry of the inclusions [24,25]. The analytical results obtained allow for the investigation of the impact of the strain field of QD on the energy band structure of the material matrix as well as within the QD itself.

The effect of the finite size of QDs on the electronic and optoelectronic properties of semiconductors has also been studied quite fully in the past decades [26,27]. In addition, it was pointed out that due to the crystal lattice mismatch between the materials of QDs and surrounding matrix, considerable elastic strains can be generated inside QDs. Such intrinsic strains contribute to the modification of semiconductor band structure via the deformation potential [10].

In this study, we briefly analyze the elastic fields of QDs in the forms of cylinder, hemisphere, and cone in nanowire. Then we use the **k·p** perturbation theory approach to investigate the influence of strain induced by $In_xGa_{1-x}N$ and $Al_yGa_{1-y}N$ QDs on the electronic band structure of the GaN matrix. Additionally, we investigate strain-induced polarization within nitride semiconductors.

2. ELASTIC FIELD OF THE QUANTUM DOT IN THE WIRE

In terms of continuum mechanics, QD can be considered as an elastic dilatational inclusion (DI) with an eigenstrain $^{DI}\varepsilon_{ii}^*$ corresponding to the mismatch between the lattice constants of the dot and the surrounding material matrix. The problem of elastic inclusion with eigenstrain in a homogeneous and isotropic elastic medium originates from the classical problem proposed by Eshelby [22,23]. In this problem, we consider a DI with an eigenstrain $^{DI}\varepsilon_{ii}^*$, defined by the following expression:

$$^{DI}\varepsilon_{ii}^* = \varepsilon^*\delta(\Omega), \tag{1}$$

where $\delta(\Omega) = \begin{cases} 1, & R \in \Omega, \\ 0, & R \notin \Omega \end{cases}$. There is no summation over i in $^{DI}\varepsilon_{ii}^*$, i is coordinate in any orthogonal coordinate system. In Eq. (1) parameter ε^* (misfit parameter) is found as ratio (see, for example [28–30])

$$\varepsilon^* = \frac{a_d - a_m}{a_m}, \tag{2}$$

where a_d and a_m are the lattice constants for QDs and surrounding material matrix in the absence of strains, respectively.

Here, we consider QDs with axial symmetry such as cylinder, cone, truncated sphere, etc. To study the elastic

properties of QDs in the nanowire, we model QDs as an infinite set of infinitesimally thin coaxial disks of radius c, uniformly distributed with a constant density ρ along the symmetrical axis. In this approach, the elastic field of QD is obtained by integrating the corresponding components of the elastic field of infinitesimal thin disks inside the nanowire, with eigenstrain $^d\varepsilon_{ii}^*$ given by following expression [24,25,31]:

$$^d\varepsilon_{ii}^* = bH\left(1-\frac{r}{c}\right)\delta(z-z_0), \tag{3}$$

where b is a coefficient with the dimension of length, $H(\zeta) = \begin{cases} 1, & \zeta \geq 0, \\ 0, & \zeta < 0 \end{cases}$ is the Heaviside step function, $\delta(z)$ is the Dirac delta function, c is the radius of the disk, and z_0 is the coordinate of disk in cylindrical coordinate system (r, φ, z); see Fig. 1. Then the elastic field of inclusion is equal to the sum of the corresponding components of the elastic field of the disks. The eigenstrain of the inclusion $^{DI}\varepsilon_{ii}^*$ can be found using eigenstrain (3) [24,25,31,32]:

$$^{DI}\varepsilon_{ii}^* = \int_{z_1}^{z_2} {}^d\varepsilon_{ii}^*(r, z-z_0)\rho dz_0$$

$$= \int_{z_1}^{z_2} bH\left(1-\frac{r}{c}\right)\delta(z-z_0)\rho dz_0 = \varepsilon^*\delta(\Omega), \tag{4}$$

where $\varepsilon^* = b\rho$.

Therefore, the elastic field of DI can be found by integration as well. For example, total displacements $^{DI}u_i$ are calculated by the following formula:

$$^{DI}u_i = \int_{z_1}^{z_2} {}^d u_i(r, z-z_0)\rho dz_0. \tag{5}$$
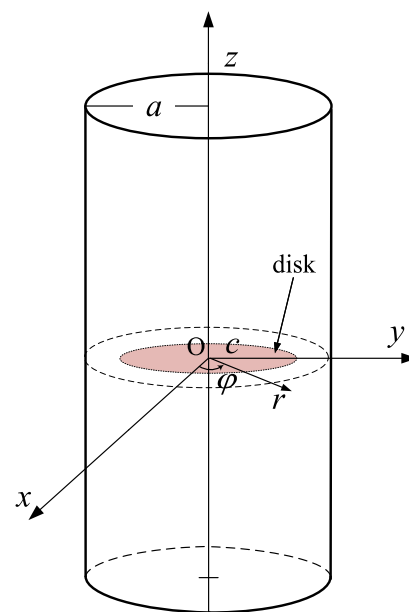
Fig. 1. The circular disk in a long cylindrical nanowire. The coordinates r, φ, z in the cylindrical coordinate system are shown.

2.1. Dilatational disk in the wire

We consider a dilatational infinitesimally thin disk (DD) (see Fig. 1) with eigenstrain $^\mathrm{d}\varepsilon_{ii}^*$ (see Eq. (3)), embedded in the circular wire:

The fields of total displacements $^\mathrm{d}u_i$, elastic strains $^\mathrm{d}\varepsilon_{ij}$ and stresses $^\mathrm{d}\sigma_{ij}$ of the DD in the cylinder are represented by the sums of the corresponding DD fields in an infinite elastic medium ($^{\infty\mathrm{d}}u_i$, $^{\infty\mathrm{d}}\varepsilon_{ij}$, $^{\infty\mathrm{d}}\sigma_{ij}$) and some additional (image) fields ($^{\mathrm{im}}u_i$, $^{\mathrm{im}}\varepsilon_{ij}$, $^{\mathrm{im}}\sigma_{ij}$) [32]:

$$^\mathrm{d}u_i = {}^{\infty\mathrm{d}}u_i + {}^{\mathrm{im}}u_i, \tag{6}$$

$$^\mathrm{d}\varepsilon_{ij} = {}^{\infty\mathrm{d}}\varepsilon_{ij} + {}^{\mathrm{im}}\varepsilon_{ij}, \tag{7}$$

$$^\mathrm{d}\sigma_{ij} = {}^{\infty\mathrm{d}}\sigma_{ij} + {}^{\mathrm{im}}\sigma_{ij}, \tag{8}$$

where $i, j = r, \varphi, z$. The detailed expressions of $^\mathrm{d}u_i$, $^\mathrm{d}\varepsilon_{ij}$, $^\mathrm{d}\sigma_{ij}$ of the disk in the wire [32]:

$$^{\infty\mathrm{d}}u_r = \frac{(1+\nu)b}{2(1-\nu)} J(1,1;0), \tag{9a}$$

$$^{\infty\mathrm{d}}u_\varphi = 0, \tag{9b}$$

$$^{\infty\mathrm{d}}u_z = \frac{(1+\nu)b}{2(1-\nu)} \operatorname{sgn}(z-z_0) J(1,0;0), \tag{9c}$$

where

$J(m,n;p) = \int_0^\infty J_m(\kappa) J_n(\kappa r/c) \exp(-\kappa|z-z_0|/c) \kappa^p d\kappa$ are the Lipschitz-Hankel integrals [33], J_m and J_n are the Bessel functions of the first kind with the corresponding argument, and ν is the Poisson's ratio.

The additional DD displacement components due to the free surface contribution of the wire [32]:

$$^{\mathrm{im}}u_r = \frac{(1+\nu)b}{(1-\nu)\pi} \int_0^\infty \left[-C\beta \frac{r}{a} I_0\left(\frac{\beta r}{a}\right) \right.$$
$$\left. + \left(4C(1-\nu) - D\beta\right) I_1\left(\frac{\beta r}{a}\right) \right] t I_1^* \cos\frac{\beta z}{a} d\beta, \tag{10a}$$

$$^{\mathrm{im}}u_\varphi = 0, \tag{10b}$$

$$^{\mathrm{im}}u_z = \frac{(1+\nu)b}{(1-\nu)\pi} \int_0^\infty \left[C\frac{r}{a} I_1\left(\frac{\beta r}{a}\right) + D I_0\left(\frac{\beta r}{a}\right) \right] \beta t I_1^* \sin\frac{\beta z}{a} d\beta, \tag{10c}$$

where

$$C = \frac{1}{\eta}, \quad D = \frac{2 - (\beta^2 - 2\nu + 2) I_1 K_1 - \beta^2 I_0 K_0 - 2\nu}{\beta\eta}, \tag{11a,b}$$

with $\eta = \beta^2 I_0^2 - (\beta^2 - 2\nu + 2) I_1^2$, $I_0 = I_0(\beta)$ and $I_1 = I_1(\beta)$ are the modified Bessel functions of the first kind, $I_1^* = I_1(t\beta)$, $t = c/a$, a is radius of the wire, $K_0 = K_0(\beta)$ and $K_1 = K_1(\beta)$ are the modified Bessel functions of the second kind (the Macdonald functions).

2.2. Cylindrical quantum dot in the wire

Consider QD in the form of a finite cylinder (CyI—cylindrical inclusion) with radius c and height h embedded in a circular nanowire with radius a (see Fig. 2).
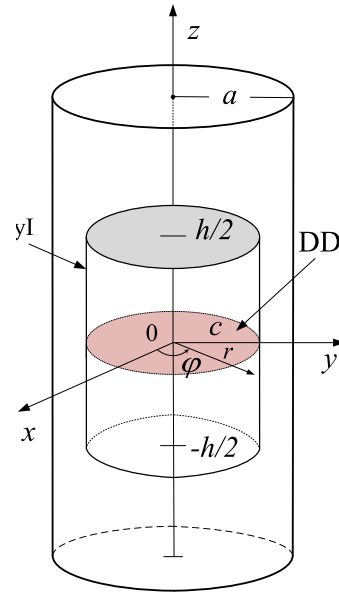
Fig. 2. A finite cylindrical quantum dot (CyI) in the circular nanowire. The coordinates r, φ, z in the cylindrical coordinate system are shown.

By substituting Eqs. (6), (9), and (10) into Eq. (5) we get the displacements of CyI in the circular nanowire. The solutions for the displacements, strains, and stresses of CyI in the circular nanowire have been found in our previous study [32,34]:

$$^{\mathrm{CyI}}u_r = {}^{\infty\mathrm{CyI}}u_r + \frac{2(1+\nu)\varepsilon^* a}{(1-\nu)\pi} \int_0^\infty \left[-C\frac{\beta r}{a} I_0\left(\frac{\beta r}{a}\right) \right.$$
$$\left. + \left(4C(1-\nu) - D\beta\right) I_1\left(\frac{\beta r}{a}\right) \right] \frac{t I_1^*}{\beta} \sin\frac{\beta h}{2a} \cos\frac{\beta z}{a} d\beta, \tag{12a}$$

$$^{\mathrm{CyI}}u_\varphi = 0, \tag{12b}$$

$$^{\mathrm{CyI}}u_z = {}^{\infty\mathrm{CyI}}u_z + \frac{2(1+\nu)\varepsilon^* a}{(1-\nu)\pi}$$
$$\times \int_0^\infty \left[C\frac{r}{a} I_1\left(\frac{\beta r}{a}\right) + D I_0\left(\frac{\beta r}{a}\right) \right] t I_1^* \sin\frac{\beta h}{2a} \sin\frac{\beta z}{a} d\beta, \tag{12c}$$

where h is the height of CyI (Fig. 2). Here other designations are the same as in Eqs. (11a,b).

The elastic strains $^{\mathrm{CyI}}\varepsilon_{ij}$ and stresses $^{\mathrm{CyI}}\sigma_{ij}$ can be determined from displacements $^{\mathrm{CyI}}u_i$ (12) according to the following relations:

• for elastic strains

$$^{\mathrm{CyI}}\varepsilon_{rr} = \frac{\partial^{\mathrm{CyI}}u_r}{\partial r} - \varepsilon^* \delta(\Omega), \tag{13a}$$

$$^{\mathrm{CyI}}\varepsilon_{\varphi\varphi} = \frac{^{\mathrm{CyI}}u_r}{r} - \varepsilon^* \delta(\Omega), \tag{13b}$$

$$^{\mathrm{CyI}}\varepsilon_{zz} = \frac{\partial^{\mathrm{CyI}}u_z}{\partial z} - \varepsilon^* \delta(\Omega), \tag{13c}$$

$$^{\mathrm{CyI}}\varepsilon_{rz} = \frac{1}{2}\left(\frac{\partial^{\mathrm{CyI}}u_r}{\partial z} + \frac{\partial^{\mathrm{CyI}}u_z}{\partial r} \right), \tag{13d}$$

$$^{\text{CyI}}\varepsilon_{r\varphi} = \frac{1}{2}\left(\frac{\partial^{\text{CyI}}u_\varphi}{\partial r} + \frac{\partial^{\text{CyI}}u_r}{\partial \varphi}\frac{1}{r} - \frac{^{\text{CyI}}u_\varphi}{r}\right), \tag{13e}$$

$$^{\text{CyI}}\varepsilon_{\varphi z} = \frac{1}{2}\left(\frac{\partial^{\text{CyI}}u_z}{\partial \varphi}\frac{1}{r} + \frac{\partial^{\text{CyI}}u_\varphi}{\partial z}\right); \tag{13f}$$

• for elastic dilatational strain:

$$^{\text{CyI}}\Delta = {^{\text{CyI}}\varepsilon_{rr}} + {^{\text{CyI}}\varepsilon_{\varphi\varphi}} + {^{\text{CyI}}\varepsilon_{zz}}; \tag{14}$$

• for stresses:

$$^{\text{CyI}}\sigma_{ij} = 2G\left(^{\text{CyI}}\varepsilon_{ij} + \frac{\nu}{1-2\nu}{^{\text{CyI}}\Delta\delta_{ij}}\right), \tag{15}$$

where $\delta_{ij} = \begin{cases} 1, & i=j, \\ 0, & i \neq j \end{cases}$ is Kronecker symbol, G is shear modulus, ν is Poisson's ratio.

The total displacements $^{\infty\text{CyI}}u_i$ of the CyI in an infinite medium were found earlier in Refs. [24,25] in the following form:

• inside the CyI ($|z|<\frac{h}{2}, r<c$)

$$^{\infty\text{CyI}}u_r^{\text{in}} = \frac{(1+\nu)\varepsilon^*c}{2(1-\nu)}\left[\frac{r}{c} - J^{(1)}(1,1;-1) - J^{(2)}(1,1;-1)\right], \tag{16a}$$

$$^{\infty\text{CyI}}u_\varphi^{\text{in}} = 0, \tag{16b}$$

$$^{\infty\text{CyI}}u_z^{\text{in}} = \frac{(1+\nu)\varepsilon^*c}{2(1-\nu)}\text{sgn}(z)\left[J^{(1)}(1,0;-1) - J^{(2)}(1,0;-1)\right]; \tag{16c}$$

• outside the CyI ($|z|>\frac{h}{2}$ or $|z|\leq\frac{h}{2}, r>c$)

$$^{\infty\text{CyI}}u_r^{\text{out}} = \frac{(1+\nu)\varepsilon^*c}{2(1-\nu)}$$

$$\times \begin{cases} J^{(3)}(1,1;-1) - J^{(2)}(1,1;-1), & |z|>\frac{h}{2}, \\ \frac{c}{r} - J^{(1)}(1,1;-1) - J^{(2)}(1,1;-1), & |z|\leq\frac{h}{2}, r>c, \end{cases} \tag{17a}$$

$$^{\infty\text{CyI}}u_\varphi^{\text{out}} = 0, \tag{17b}$$

$$^{\infty\text{CyI}}u_z^{\text{out}} = \frac{(1+\nu)\varepsilon^*c}{2(1-\nu)}\text{sgn}(z)$$

$$\times \begin{cases} J^{(3)}(1,0;-1) - J^{(2)}(1,0;-1), & |z|>\frac{h}{2}, \\ J^{(1)}(1,0;-1) - J^{(2)}(1,0;-1), & |z|\leq\frac{h}{2}, r>c. \end{cases} \tag{17c}$$

Here the Lipschitz-Hankel integrals $J^{(l)}(m,n;p) = \int_0^\infty J_m(\kappa)J_n(\kappa r/c)e^{-\kappa\xi_l}\kappa^p d\kappa$ with $l=1, 2, 3$, are used with $\xi_1 = (\frac{h}{2}-|z|)/c$, $\xi_2 = (\frac{h}{2}+|z|)/c$, and $\xi_3 = (|z|-\frac{h}{2})/c$.

From the expressions obtained for the displacements (13), (16), and (17) of CyI we can easily determine the strains as well as the hydrostatic strain. The total hydrostatic strain is determined by the following expression:

$$^{\text{CyI}}\Delta = \frac{\partial^{\text{CyI}}u_r}{\partial r} + \frac{^{\text{CyI}}u_r}{r} + \frac{\partial^{\text{CyI}}u_z}{\partial z} = \frac{(1+\nu)\varepsilon^*}{1-\nu}$$

$$\times\left[\delta(\Omega) + \frac{4}{\pi}\int_0^\infty (1-2\nu)CI_0(\frac{\beta r}{a})tI_1^*\sin(\frac{\beta h}{2a})\cos(\frac{\beta z}{a})d\beta\right]. \tag{18}$$

Contour plots of the total hydrostatic strains induced by CyI in the nanowire are shown in Fig. 3.
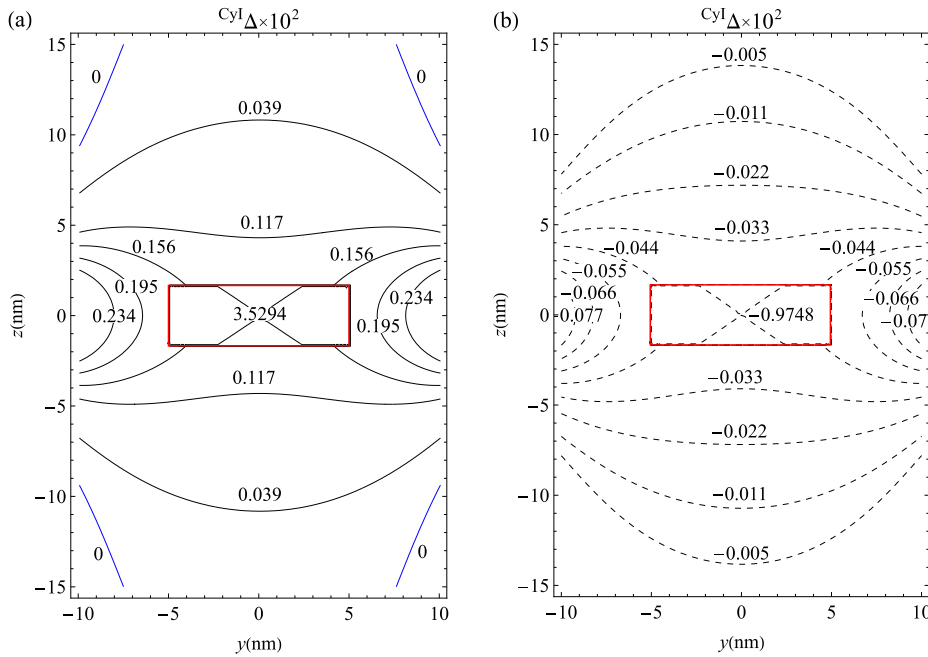
Fig. 3. The total hydrostatic strain maps of the CyI in a circular nanowire: (a) $In_{0.2}Ga_{0.8}N$ dot in GaN matrix and (b) $Al_{0.2}Ga_{0.8}N$ dot in GaN matrix. The parameters used for calculations are as follows: nanowire radius $a = 10$ nm; the base radius and height of CyI are $c = 5$ nm and $h = 10/3$ nm, respectively; the Poisson's ratio of GaN $\nu = 0.234$; misfit parameters of $In_{0.2}Ga_{0.8}N$ and $Al_{0.2}Ga_{0.8}N$ dots are $\varepsilon^* = 0.021$ and -0.0058, respectively.
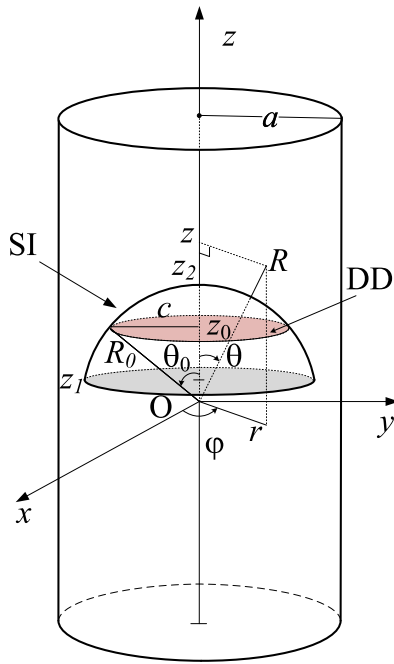
Fig. 4. The truncated spherical quantum dot (SI) with radius R_0 embedded in the circular nanowire with radius a. The cylindrical coordinates r, φ, z are shown.

2.3. Truncated spherical quantum dot in the nanowire

QDs in truncated spherical form also frequently appear in the fabrication of nanomaterials. We consider a truncated spherical quantum dot (SI) with a radius R_0 ($\theta_1 < \theta_0 < \theta_2$) coaxially buried in the circular nanowire with radius a and infinite length (Fig. 4). The eigenstrain $^{DI}\varepsilon_{ii}^*$ of SI defined according to Eq. (1).

Then it can be considered that QDs are formed from infinitesimal dilatational thin disks with the radius varying according to a specific rule $c = R_0 \sin\theta_0$ [25] and distributed along the symmetrical axis of the disk with constant density ρ. The displacements $^{SI}u_i$ of SI obtained by substituting Eqs. (6), (9), and (10) into Eq. (5). The displacement components of SI in infinite space can be found in Ref. [25]. The additional parts of the displacements of SI are calculated according to the following expressions:

$$^{SI}u_r = {}^{\infty SI}u_r + \frac{(1+\nu)\varepsilon^*}{(1-\nu)\pi}$$

$$\times \int_0^\infty \left[-C\frac{\beta r}{a} I_0\left(\frac{\beta r}{a}\right) + \left(4C(1-\nu) + D\beta\right) I_1\left(\frac{\beta r}{a}\right) \right] d\beta$$

$$\times \int_{z_1}^{z_2} t\, I_1(\beta t)\cos\frac{\beta(z-z_0)}{a} dz_0, \tag{19a}$$

$$^{SI}u_\varphi = 0, \tag{19b}$$

$$^{SI}u_z = {}^{\infty SI}u_z + \frac{(1+\nu)\varepsilon^*}{(1-\nu)\pi}\int_0^\infty \left[C\frac{r}{a} I_1\left(\frac{\beta r}{a}\right) + D I_0\left(\frac{\beta r}{a}\right) \right]\beta d\beta$$

$$\times \int_{z_1}^{z_2} t I_1(\beta t)\sin\frac{\beta(z-z_0)}{a} dz_0. \tag{19c}$$

Coefficients C and D are determined according to Eqs. (11), (12) and $t = c/a$. To calculate the integrals: $\int_{z_1}^{z_2} t I_1(\beta t)\cos\frac{\beta(z-z_0)}{a} dz_0$ and $\int_{z_1}^{z_2} t I_1(\beta t)\sin\frac{\beta(z-z_0)}{a} dz_0$ let us express the modified Bessel functions of the first kind $I_n(x)$ [35], $\sin(x)$ and $\cos(x)$ in the form of a series

$$\int_{z_1}^{z_2} t I_1(\beta t)\cos\frac{\beta(z-z_0)}{a} dz_0 = A\cos\frac{\beta z}{a} + \Lambda\sin\frac{\beta z}{a}, \tag{20a}$$

$$\int_{z_1}^{z_2} t I_1(\beta t)\sin\frac{\beta(z-z_0)}{a} dz_0 = A\sin\frac{\beta z}{a} - \Lambda\cos\frac{\beta z}{a}, \tag{20b}$$

with

$$A = R_0 \sum_{k=0}^\infty \frac{\beta^{1+2k}}{2^{1+2k} k!(k+1)!}\left(\frac{R_0}{a}\right)^{2k+2}$$

$$\times \sum_{m=0}^\infty \frac{(-1)^m \beta^{2m}}{(2m)!}\left(\frac{R_0}{a}\right)^{2m} \int_{\mu_1}^{\mu_2} \mu_0^{2m}(1-\mu_0^2)^{k+1} d\mu_0, \tag{21a}$$

$$\Lambda = R_0 \sum_{k=0}^\infty \frac{\beta^{1+2k}}{2^{1+2k} k!(k+1)!}\left(\frac{R_0}{a}\right)^{2k+2}$$

$$\times \sum_{m=0}^\infty \frac{(-1)^m \beta^{2m+1}}{(2m+1)!}\left(\frac{R_0}{a}\right)^{2m+1} \int_{\mu_1}^{\mu_2} \mu_0^{2m+1}(1-\mu_0^2)^{k+1} d\mu_0, \tag{21b}$$

where $\mu_0 = \cos\theta_0$, $\mu = \cos\theta$, $\mu_1 = \cos\theta_1$, $\mu_2 = \cos\theta_2$, $z = R\mu$, $z_0 = R_0\mu_0$,

$$\int_{\mu_1}^{\mu_2} \mu_0^{2m}(1-\mu_0^2)^{k+1} d\mu_0 = \frac{1}{2}\begin{cases} -B_{\mu_1^2}(m+\frac{1}{2}, k+2) + B_{\mu_2^2}(m+\frac{1}{2}, k+2), & 0 < \mu_1 < \mu_2 < 1, \\ B_{\mu_1^2}(m+\frac{1}{2}, k+2) - B_{\mu_2^2}(m+\frac{1}{2}, k+2), & -1 < \mu_1 < \mu_2 < 0, \\ B_{\mu_1^2}(m+\frac{1}{2}, k+2) + B_{\mu_2^2}(m+\frac{1}{2}, k+2), & -1 < \mu_1 < 0 \text{ and } 0 < \mu_2 < 1, \end{cases}$$

$$\int_{\mu_1}^{\mu_2} \mu_0^{2m+1}(1-\mu_0^2)^{k+1} d\mu_0 = \frac{1}{2}\left[-B_{\mu_1^2}(m+1, k+2) + B_{\mu_2^2}(m+1, k+2) \right],$$

and $B_\mu(m,k) = \int_0^\mu x^{m-1}(1-x)^{k-1} dx$ is the incomplete Beta function [36].

The displacements of the SI in an infinite medium $^{\infty SI}u_i$ can be written in the following form [25]:

• inside sphere ($R < R_0$)

$$^{\infty SI}u_r\big|_{R<R_0} = \frac{(1+\nu)\varepsilon^* R_0}{2(1-\nu)} \sum_{k=1}^\infty \frac{P_k^1(\mu)}{k(k+1)} \frac{R^k}{R_0^k} L_k, \qquad (22a)$$

$$^{\infty SI}u_\varphi\big|_{R<R_0} = 0, \qquad (22b)$$

$$^{\infty SI}u_z\big|_{R<R_0} = \frac{(1+\nu)\varepsilon^* R_0}{2(1-\nu)}$$

$$\times \left[\left\{ \begin{array}{l} \frac{z_2-z_1}{R_0}, z > z_2 \\ \frac{z_1-z_2}{R_0}, z < z_1 \\ \frac{2z-z_1-z_2}{R_0}, z_1 < z < z_2 \end{array} \right\} + \frac{1}{2}(\mu_2^2 - \mu_1^2) + \sum_{k=1}^\infty \frac{1}{k} \frac{R^k}{R_0^k} P_k(\mu) L_k \right], \qquad (22c)$$

• outside sphere ($R > R_0$)

$$^{\infty SI}u_r\big|_{R>R_0} = \frac{(1+\nu)\varepsilon^* R_0}{2(1-\nu)} \sum_{k=1}^\infty \frac{1}{k(k+1)} \frac{R_0^{k+1}}{R^{k+1}} P_k^1(\mu) L_k, \qquad (23a)$$

$$^{\infty SI}u_\varphi\big|_{R>R_0} = 0, \qquad (23b)$$

$$^{\infty SI}u_z\big|_{R>R_0} = -\frac{(1+\nu)\varepsilon^* R_0}{2(1-\nu)} \sum_{k=1}^\infty \frac{1}{k+1} \frac{R_0^{k+1}}{R^{k+1}} P_k(\mu) L_k, \qquad (23c)$$

where

$$L_k = \frac{k(k+1)}{2k+1} \left[\frac{P_{k-2}(\mu_1) - P_k(\mu_1) - P_{k-2}(\mu_2) + P_k(\mu_2)}{1-2k} \right.$$

$$\left. + \frac{P_k(\mu_1) - P_{k+2}(\mu_1) - P_k(\mu_2) + P_{k+2}(\mu_2)}{2k+3} \right];$$

$z_1 = R_0 \cos\theta_1$, $z_2 = R_0 \cos\theta_2$; $P_k(\mu)$ are Legendre polynomials; associated Legendre polynomials are defined as $P_n^1(\mu) = (-1)(1-\mu^2)^{1/2} dP_n(\mu)/d\mu$.

From the Eqs. (19), (22), and (23) of displacements we can determine the strain, stresses, and total hydrostatic strain of the dot by using the Eqs. (14), (15). The total hydrostatic strain of SI is determined by the following expression:

$$^{SI}\Delta = \frac{\partial^{SI}u_r}{\partial r} + \frac{^{SI}u_r}{r} + \frac{\partial^{SI}u_z}{\partial z} = \frac{(1+\nu)\varepsilon^*}{1-\nu}$$

$$\times \left[\delta(\Omega) + \frac{2(1-2\nu)}{\pi a} \int_0^\infty C I_0\left(\frac{\beta r}{a}\right) \left(A\cos\frac{\beta z}{a} + \Lambda\sin\frac{\beta z}{a} \right) \beta d\beta \right], \qquad (24)$$

where A and Λ are functions of β determined by Eqs. (21a,b). The total hydrostatic strain contour maps of the hemispherical dot are shown in Fig. 5.

2.4. Conical quantum dot in the circular nanowire

Consider a conical quantum dot (CI—conical inclusion) embedded in the circular nanowire, as shown in Fig. 6, with eigenstrain $^{DI}\varepsilon_{ii}^*$ defined according to Eq. (1). To determine the displacements, strains, and stresses of the dot, we use the same approach as for CyI and SI in nanowire (see Sections 2.2 and 2.3). In this method, the quantum dot is modeled by thin circular disks with eigenstrain, defined by Eq. (3) with a radius of $c = R_0\sin\theta_0$, with $\theta_0 = \text{const}$, and radius R_0 varying according to the position z_0 of the
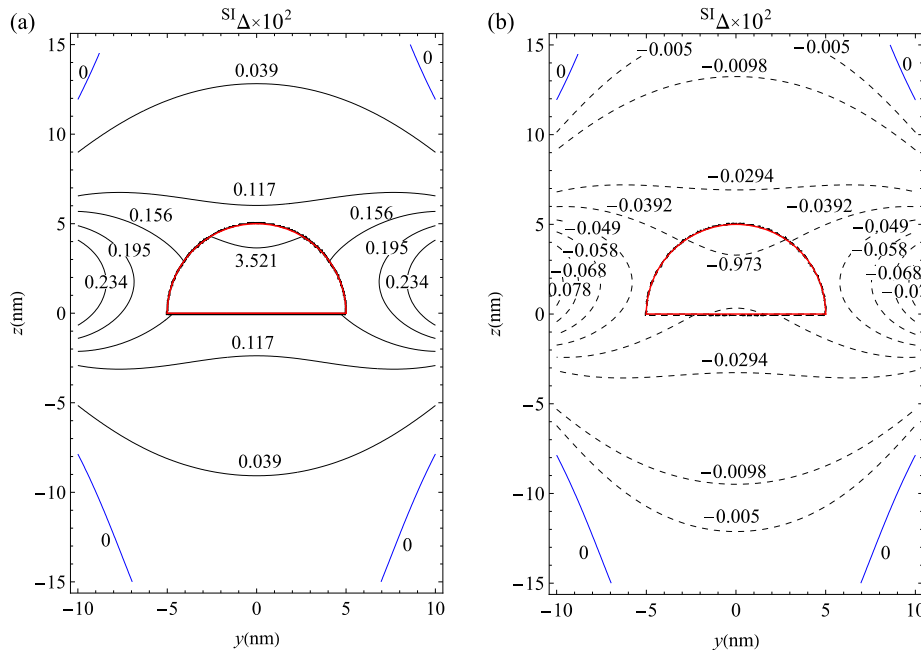
Fig. 5. The total hydrostatic strain maps of hemispherical QD in the circular nanowire: (a) In$_{0.2}$Ga$_{0.8}$N dot in GaN nanowire, (b) Al$_{0.2}$Ga$_{0.8}$N dot in GaN nanowire. The parameters used for the calculations: nanowire radius $a = 10$ nm, radius of the sphere $R_0 = 5$ nm, Poisson's ratio of GaN $\nu = 0.234$; misfit parameters of In$_{0.2}$Ga$_{0.8}$N and Al$_{0.2}$Ga$_{0.8}$N dots are $\varepsilon^* = 0.021$ and -0.0058, respectively.
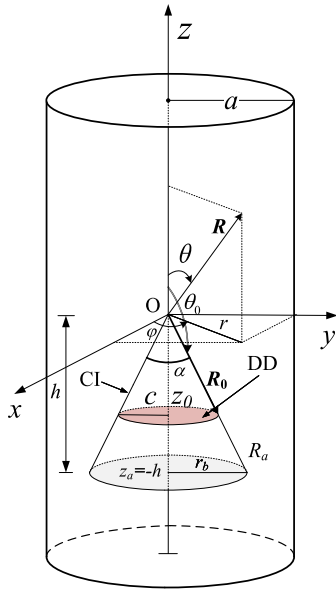
Fig. 6. The conical QD with height h and base radius r_b is embedded in the circular nanowire with radius a. The coordinates in the cylindrical coordinate system r, φ.

disks (see Fig. 6). The total displacements of CI are determined from disks by substituting Eqs. (6), (9), and (10) into Eq. (5).

The displacement components corresponding to CI in infinite space have been previously studied in our earlier research [37]. The additional displacement components due to the contribution of the nanowire's free surface condition are determined by the following expressions:

$$^{CI}u_r = {}^{\infty CI}u_r + \frac{(1+\nu)\varepsilon^*}{(1-\nu)\pi}$$

$$\times \int_0^\infty \left[-C\frac{\beta r}{a}I_0\left(\frac{\beta r}{a}\right) + \left(4C(1-\nu)+D\beta\right)I_1\left(\frac{\beta r}{a}\right)\right]d\beta$$

$$\times \int_{-h}^0 t\,I_1(\beta t)\cos\frac{\beta(z-z_0)}{a}dz_0 \,, \qquad (25a)$$

$$^{CI}u_\varphi = 0, \qquad (25b)$$

$$^{CI}u_z = {}^{\infty CI}u_z + \frac{(1+\nu)\varepsilon^*}{(1-\nu)\pi}\int_0^\infty\left[C\frac{r}{a}I_1\left(\frac{\beta r}{a}\right) + D\,I_0\left(\frac{\beta r}{a}\right)\right]\beta\,d\beta$$

$$\times \int_{-h}^0 t\,I_1(\beta t)\sin\frac{\beta(z-z_0)}{a}dz_0. \qquad (25c)$$

To calculate the integrals $\int_{-h}^0 t\,I_1(\beta t)\cos\dfrac{\beta(z-z_0)}{a}dz_0$ and $\int_{-h}^0 t\,I_1(\beta t)\sin\dfrac{\beta(z-z_0)}{a}dz_0$, let us express the modified Bessel functions $I_n(x)$ [35], $\sin(x)$, $\cos(x)$ in the form of a series. We have

$$\int_{-h}^0 t\,I_1(\beta t)\cos\frac{\beta(z-z_0)}{a}dz_0 = \Xi\cos\frac{\beta z}{a} - \Theta\sin\frac{\beta z}{a},$$

$$\int_{-h}^0 t\,I_1(\beta t)\sin\frac{\beta(z-z_0)}{a}dz_0 = \Xi\sin\frac{\beta z}{a} + \Theta\cos\frac{\beta z}{a},$$

with

$$\Xi = h\sum_{n=0}^\infty \frac{(-1)^n}{(2n)!}\frac{\tan^2\theta_0}{2(2n+3)}\left(\frac{h}{a}\right)^{2n+2}$$

$$\times {}_1F_2\left(n+\frac{3}{2};2,n+\frac{5}{2};\frac{r_b^2\beta^2}{4a^2}\right)\beta^{2n+1}, \qquad (26a)$$

$$\Theta = h\sum_{n=0}^\infty \frac{(-1)^n}{(2n+1)!}\frac{\tan^2\theta_0}{4(n+2)}\left(\frac{h}{a}\right)^{2n+3}$$

$$\times {}_1F_2\left(n+2;2,n+3;\frac{r_b^2\beta^2}{4a^2}\right)\beta^{2n+2}, \qquad (26b)$$

where ${}_mF_n(c_1,c_2,...,c_m;d_1,d_2,...,d_n;x)$ is the generalized hypergeometric function [38] which can be written via series:

$${}_mF_n(c_1,c_2,...,c_m;d_1,d_2,...,d_n;x) = \sum_{k=0}^\infty \frac{(c_1)_k...(c_m)_k}{(d_1)_k...(d_n)_k}\frac{x^k}{k!}.$$

Here $(c)_k$ and $(d)_k$ are Pochhammer symbols

$$(c)_k = c(c+1)...(c+k-1) = \frac{\Gamma(c+k)}{\Gamma(c)},$$

$$(d)_k = d(d+1)...(d+k-1) = \frac{\Gamma(d+k)}{\Gamma(d)},$$

with $\Gamma(z) = \int_0^\infty t^{z-1}e^{-t}dt$ is Gamma function.

The displacements ${}^{\infty CI}u_i$ of the CI in an infinite medium were found in Ref. [37] in the following form:

• for $R < R_a$

$$^{\infty CI}u_r\Big|_{R<R_a} = \frac{(1+\nu)\varepsilon^*R_a}{2(1-\nu)}\left[-\frac{R}{R_a}\mu_0\sqrt{1-\mu_0^2}\sum_{k=1}^\infty\frac{P_k^1(\mu)P_k^1(\mu_0)}{k(k+1)(k+2)}\right.$$

$$-\frac{1}{2}\frac{R}{R_a}\mu_0(1-\mu_0^2)\sqrt{1-\mu^2}\log\frac{R_a}{R}$$

$$\left. +\frac{R}{R_a}\mu_0\sqrt{1-\mu_0^2}\sum_{k=2}^\infty\frac{P_k^1(\mu)P_k^1(\mu_0)}{(k-1)k(k+1)}(R^{k-1}/R_a^{k-1}-1)\right], \quad (27a)$$

$$^{\infty CI}u_\varphi = 0, \qquad (27b)$$

$$^{\infty CI}u_z\Big|_{R<R_a} = \frac{(1+\nu)\varepsilon^*R_a}{2(1-\nu)}\left[\frac{R}{R_a}\mu_0\sqrt{1-\mu_0^2}\sum_{k=1}^\infty\frac{P_k^1(\mu_0)P_k(\mu)}{(k+1)(k+2)}\right.$$

$$+\frac{1}{R_a}\begin{Bmatrix}2z-R_a\mu_0-R\mu_0, z_a<z<R\mu_0\\ -R_a\mu_0+R\mu_0, z_a<R\mu_0<z\\ R_a\mu_0-R\mu_0, z<z_a<R\mu_0\end{Bmatrix}$$

$$-\mu_0^2(1-R/R_a)+\frac{R}{R_a}\mu_0\mu(1-\mu_0^2)\log\frac{R_a}{R}$$

$$\left. -\frac{R}{R_a}\mu_0\sqrt{1-\mu_0^2}\sum_{k=2}^\infty\frac{P_k^1(\mu_0)P_k(\mu)}{k(1-k)}(R^{k-1}/R_a^{k-1}-1)\right], \quad (27c)$$

• for $R > R_a$

$$^{\infty CI}u_r\Big|_{R>R_a} = -\frac{(1+\nu)\varepsilon^*R_a}{2(1-\nu)}\mu_0\sqrt{1-\mu_0^2}\sum_{k=1}^\infty\frac{P_k^1(\mu)P_k^1(\mu_0)}{k(k+1)(k+2)}\left(\frac{R_a}{R}\right)^{k+1},$$

$$(28a)$$
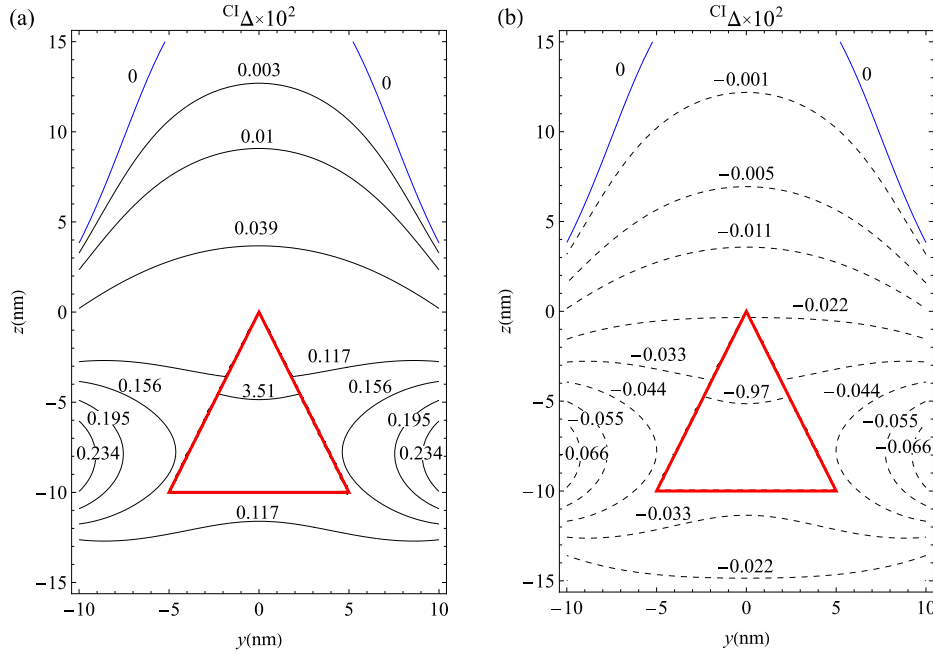
Fig. 7. The total hydrostatic strain maps of CI in the nanowire, (a) $In_{0.2}Ga_{0.8}N$ dot in GaN matrix; (b) $Al_{0.2}Ga_{0.8}N$ dot in GaN nanowire. The parameters used for the calculations: the radius of the nanowire $a = 10$ nm, the base radius and height of CI are $r_b = 5$ nm and $h = 10$ nm, respectively; the Poisson's ratio of GaN $\nu = 0.234$; misfit parameters of $In_{0.2}Ga_{0.8}N$ and $Al_{0.2}Ga_{0.8}N$ dots are $\varepsilon^* = 0.021$ and -0.0058, respectively.

$$^{\infty CI}u_\varphi = 0, \tag{28b}$$

$$^{\infty CI}u_z\big|_{R>R_a} = \frac{(1+\nu)\varepsilon^* R_a}{2(1-\nu)}\mu_0\sqrt{1-\mu_0^2}\sum_{k=1}^{\infty}\frac{P_k^1(\mu_0)P_k(\mu)}{(k+1)(k+2)}\left(\frac{R_a}{R}\right)^{k+1}. \tag{28c}$$

where $R_a = r_b/\sin(\alpha/2)$, with α is the opening angle of the cone.

Then we can calculate strains and stresses of QD by substituting Eqs. (25), (27), and (28) into Eqs. (14), (15). The total hydrostatic strain of conical QD in nanowire is determined by the following expression

$$^{CI}\Delta = \frac{\partial\,^{CI}u_r}{\partial r} + \frac{^{CI}u_r}{r} + \frac{\partial\,^{CI}u_z}{\partial z} = \frac{(1+\nu)\varepsilon^*}{(1-\nu)}\left[\frac{2(2\nu-1)}{1+\nu}\delta(\Omega)\right.$$
$$\left. + \frac{1}{\pi a}\int_0^{\infty} CI_0\left(\frac{\beta r}{a}\right)\left(\Xi\cos\frac{\beta z}{a} + \Theta\sin\frac{\beta z}{a}\right)\beta d\beta\right]. \tag{29}$$

where Ξ, Θ are functions of β determined by Eqs. (26a,b). The total hydrostatic strains of CI corresponding to $In_{0.2}Ga_{0.8}N$ and $Al_{0.2}Ga_{0.8}N$ dots are shown in Fig. 7.

To conveniently investigate the influence of strains on the electronic band structure and piezoelectric polarization of semiconductors, we need to represent strains in the Cartesian coordinate system according to the following relations [39]:

$$\varepsilon_{xx} = \frac{x^2\varepsilon_{rr} - 2xy\varepsilon_{r\varphi} + y^2\varepsilon_{\varphi\varphi}}{x^2+y^2}, \tag{30a}$$

$$\varepsilon_{yy} = \frac{y^2\varepsilon_{rr} + 2xy\varepsilon_{r\varphi} + x^2\varepsilon_{\varphi\varphi}}{x^2+y^2}, \tag{30b}$$

$$\varepsilon_{zz} = \varepsilon_{zz}, \tag{30c}$$

$$\varepsilon_{xy} = \frac{1}{x^2+y^2}(x^2\varepsilon_{r\varphi} - y^2\varepsilon_{r\varphi} + xy(\varepsilon_{rr} - \varepsilon_{\varphi\varphi})), \tag{30d}$$

$$\varepsilon_{yz} = \frac{y\varepsilon_{rz} + x\varepsilon_{\varphi z}}{\sqrt{x^2+y^2}}, \tag{30e}$$

$$\varepsilon_{xz} = \frac{x\varepsilon_{rz} - y\varepsilon_{\varphi z}}{\sqrt{x^2+y^2}}. \tag{30f}$$

3. EFFECT OF THE STRAIN ON CONDUCTION AND VALENCE BAND

In this study, the dilatational $In_xGa_{1-x}N$ and $Al_yGa_{1-y}N$ QDs are buried in the GaN nanowire. Due to the difference between the lattice constants of QDs and the matrix, QDs will deform the lattice of the GaN matrix. This lattice deviation changes the lattice parameters and crystal symmetry, thereby changing the electronic band structure of the matrix and QDs itself [40–42]. In general, the effect of strain on the electronic band structure of semiconductors is described using the approach proposed by Bir and Pikus [10], which uses $\mathbf{k}\cdot\mathbf{p}$ perturbation theory to study the change in electronic band structure compared to unstrained crystals. The $\mathbf{k}\cdot\mathbf{p}$ perturbation theory formalism is based on the Bloch solution of the Schrodinger equation of $\psi_{n\mathbf{k}}(\mathbf{r}) = u_{n\mathbf{k}}(\mathbf{r})\exp(i\mathbf{k}\cdot\mathbf{r})$, where n and $\mathbf{k}$ are the band index and wave vector of the electron, respectively. Substituting the Bloch functions into the Schrodinger equation, the Hamiltonian operator for the unit cell wave function can

be written as a sum of the Hamiltonian for the case $\mathbf{k} = 0$ and the term is proportional to $\mathbf{k} \cdot \mathbf{p}$ with $\mathbf{p} = \frac{\hbar}{i}\nabla$. Furthermore, the set of functions $u_{n0}(\mathbf{r})$ forms a complete set of eigenfunctions, so all eigenfunctions $u_{nk}(\mathbf{r})$ can be written as linear combination of all $u_{n0}(\mathbf{r})$, also called the Luttinger-Kohn representation [43,44]. Therefore, it is possible to apply first-order perturbation theory, with perturbations $\mathbf{k} \cdot \mathbf{p}$ and basis $u_{n0}(\mathbf{r})$. Bir and Pikus [10] demonstrated that the strain-dependent form of the Hamiltonian is essentially the same as the $\mathbf{k}$-dependent form of the Hamiltonian.

In unstrained wurtzite GaN, there are three closely spaced top valence bands (VB) at the center of the Brillouin zone, commonly referred to as heavy-hole (HH), light-hole (LH), and crystal-field split-off hole (CH) [44–46]. These VB states have atomic p-orbital character, in contrast to the bottom conduction band (CB), which has atomic s-orbital character. Since the large band gap of GaN reduces the interaction of CB and VB states, the Hamiltonian for the strain dependence of the VB can be separately given by the 6×6 matrix [10,46]:

$$\boldsymbol{H}^v(k,\varepsilon) = \begin{pmatrix} F & 0 & -H^* & 0 & K^* & 0 \\ 0 & G & \Delta & -H^* & 0 & K^* \\ -H & \Delta & \lambda & 0 & I^* & 0 \\ 0 & -H & 0 & \lambda & \Delta & I^* \\ K & 0 & I & \Delta & G & 0 \\ 0 & K & 0 & I & 0 & F \end{pmatrix}. \quad (31)$$

Here:

$\Delta = \sqrt{2}\Delta_3$; $F = \Delta_1 + \Delta_2 + \lambda + \theta$; $G = \Delta_1 - \Delta_2 + \lambda + \theta$;
$K = A_5 k_+^2 + D_5 \varepsilon_+$; $H = i(A_6 k_z k_+ + A_7 k_+ + D_6 \varepsilon_{z+})$;
$I = i(A_6 k_z k_+ - A_7 k_+ + D_6 \varepsilon_{z+})$;
$\lambda = A_1 k_z^2 + A_2 k_\perp^2 + D_1 \varepsilon_{zz} + D_2(\varepsilon_{xx} + \varepsilon_{yy})$;
$\theta = A_3 k_z^2 + A_4 k_\perp^2 + D_3 \varepsilon_{zz} + D_4(\varepsilon_{xx} + \varepsilon_{yy})$,
$k_\pm = k_x \pm ik_y$, $k_\perp^2 = k_x^2 + k_y^2$, $k_\pm = k_x \pm ik_y$,
$\varepsilon_{z\pm} = \varepsilon_{xz} \pm i\varepsilon_{yz}$, $\varepsilon_\pm = \varepsilon_{xx} - \varepsilon_{yy} \pm 2i\varepsilon_{xy}$, $\varepsilon_\perp = \varepsilon_{xx} + \varepsilon_{yy}$,

where parameters D_j ($j = 1,2,…,6$) denote the deformation potentials VB, and A_j ($j = 1,2,…,7$) are equivalent to the Luttinger parameters [44], parameter Δ_1 is the crystal-field parameter, while Δ_2 and Δ_3 are the spin-orbit energy parameters. The values of D_j, Δ_1, Δ_2, Δ_3 for GaN with wirtzite structure are listed in Table 1. The basis for conventional $\boldsymbol{H}^v$ is chosen as [45]:

$$u_1 = -\frac{1}{\sqrt{2}}|X+iY,\alpha\rangle, \; u_2 = \frac{1}{\sqrt{2}}|X-iY,\alpha\rangle, \; u_3 = |Z,\alpha\rangle,$$
$$(32a–c)$$
$$u_4 = \frac{1}{\sqrt{2}}|X-iY,\beta\rangle, \; u_5 = -\frac{1}{\sqrt{2}}|X+iY,\beta\rangle, \; u_6 = |Z,\beta\rangle,$$
$$(32d–f)$$

here, $|X\rangle$, $|Y\rangle$, and $|Z\rangle$ have the symmetry properties of the atomic p_x, p_y, and p_z orbital functions. $|\alpha\rangle$ and $|\beta\rangle$ de-

Table 1. Band structure parameters for wurtzite GaN [47].

Parameters	Values (eV)
E_g	3.479
Δ_{cr}	0.010
Δ_{SO}	0.015
$\Delta_1 = \Delta_{cr}$	0.022
$\Delta_2 = \Delta_3 = \Delta_{SO}/3$	0.005
$\alpha_\parallel$	−44.5
$\alpha_\perp$	−44.5
D_1	−41.4
D_2	−33.3
D_3	8.2
D_4	−4.1
D_5	−4.7
D_6	−7.5

note the spin wave functions corresponding to spin up and spin down, respectively. The diagonalization of the matrix (31) yields the three distinct VB maxima $E_{v,j}$.

The Hamiltonian for the strain dependence of CB minimum is given by a 2×2 matrix with basis $|S,\alpha\rangle$ and $|S,\beta\rangle$. Its single distinct eigenvalue E_c (due to strain) can be expressed as [44,47]

$$E_c = \frac{\hbar^2 k_z^2}{2m_e^\parallel} + \frac{\hbar^2(k_x^2 + k_y^2)}{2m_e^\perp} + \alpha_\parallel \varepsilon_{zz} + \alpha_\perp(\varepsilon_{xx} + \varepsilon_{yy}), \quad (33)$$

where k_x, k_y, k_z are x, y, z-components of wave vector; $\alpha_\perp$, $\alpha_\parallel$ and $m_{e\parallel}$, $m_{e\perp}$ denote the CB deformation potentials and electron effective mass, respectively. Here we only consider the ground energy state ($\mathbf{k} = 0$), so Eq. (33) is reduced to the following expression

$$E_c|_{\mathbf{k}=0} = \alpha_\parallel \varepsilon_{zz} + \alpha_\perp(\varepsilon_{xx} + \varepsilon_{yy}). \quad (34)$$

The values of $\alpha_\parallel$ and $\alpha_\perp$ for GaN with wurtzite structure are listed in Table 1.

4. POLARIZATION EFFECTS IN NITRIDE SEMICONDUCTORS

For the wurtzite structure the arrangement is ABABAB along the [0001] direction, while for the zincblende structure the arrangement is ABCABC along the [001] direction, where A, B, and C refer to allowed sites of the III-N pairs of the closed-packed layers [48].

The presence of electric polarization is directly related to the symmetry of the crystals, for the wurtzite structure each group-III is tetrahedral coordinated to four nitrogen atoms. In the absence of an external electric field, macroscopic polarization is the sum of the spontaneous polarization of the equilibrium structure P^{sp} and the strain-induced polarization P^{pz}. Nitride semiconductors with wurtzite structure exhibit a single polar axis, namely the [0001] axis. Therefore, the wurtzite phase has a

spontaneous electrical polarization along the [0001] direction even when in equilibrium, which is different from the mixed semiconductors with a zinc mixed structure. Because of the appearance of strain around QDs due to lattice deflection such deformation of the unit cell leads to additional piezoelectric polarization. By considering the symmetry of the P6$_3$mc space group of wurtzite III-nitrides, the piezoelectric polarization is related to the deformation, which is expressed by the following expression [48]:

$$P^{pz} = \begin{pmatrix} 0 & 0 & 0 & 0 & e_{15} & 0 \\ 0 & 0 & 0 & e_{15} & 0 & 0 \\ e_{31} & e_{31} & e_{33} & 0 & 0 & 0 \end{pmatrix} \begin{pmatrix} \varepsilon_{xx} \\ \varepsilon_{yy} \\ \varepsilon_{zz} \\ \varepsilon_{yz} \\ \varepsilon_{xz} \\ \varepsilon_{xy} \end{pmatrix}$$

$$= \begin{pmatrix} e_{15}\varepsilon_{xz} \\ e_{15}\varepsilon_{yz} \\ e_{31}(\varepsilon_{xx} + \varepsilon_{yy}) + e_{33}\varepsilon_{zz} \end{pmatrix}, \tag{35}$$

with the elements e_{ij} of the piezoelectric tensor in Voigt notation; see Ref. [49]. For example, values of elements of the piezoelectric tensor of III-nitride are shown in Table 2. We note that the relations of Eq. (35) are given in the natural N-coordinate system relative to the c axis. Any spatial variation in total polarization **P** leads to a fixed volume charge density:

$$\rho = -\nabla \cdot \mathbf{P}, \tag{36}$$

where $\nabla = \mathbf{i}\dfrac{\partial}{\partial x} + \mathbf{j}\dfrac{\partial}{\partial y} + \mathbf{k}\dfrac{\partial}{\partial z}$ is divergence operator.

For the step change in polarization at the interface, Eq. (36) is modified to give the fixed surface charge density [41]

$$q = -\mathbf{n} \cdot \Delta\mathbf{P}, \tag{37}$$

where **n** is the normal vector to the free surface or interface, and $\Delta\mathbf{P}$ is the total polarization change.

Table 2. Piezoelectric coefficients (given in C·m^{-2}) of GaN with the wurtzite structure [29].

Piezoelectric coefficients	GaN
e_{33}	0.73
e_{31}	−0.49
e_{15}	−0.40

Table 3. Crystal lattice parameters (given in Å) of III-nitrides with wurtzite structure (at 300 K) [52].

Lattice parameters	AlN	GaN	InN
a	3.112	3.189	3.533
c	4.982	5.186	5.693

5. DESCRIPTION OF THE MODEL

In this study, we consider In$_x$Ga$_{1-x}$N or Al$_y$Ga$_{1-y}$N QDs in the form of finite cylinder, truncated sphere, and cone in the circular nanowire, as shown in Fig. 8.

In our model, In$_x$Ga$_{1-x}$N, Al$_y$Ga$_{1-y}$N QDs, with x and y varying in the range of 0.2 to 0.5, are embedded in a circular GaN nanowire with a radius of a = 10 nm. The selected QDs have a volume of $250\pi/3$ nm^3 and radius of base of the dots r_b = 5 nm.

The effective misfit parameter f for wurtzite semiconductors can be estimated by considering the difference in crystal lattice translations in the basal plane and in the z-axis direction. The lattice parameters of III-nitrides are given in Table 3. For such materials, one can introduce a pair of misfit parameters f_a and f_c, given by

$$f_a = \frac{a_d - a_m}{a_m}, \quad f_c = \frac{c_d - c_m}{c_m}, \tag{38a,b}$$

where a_m, a_d, and c_m, c_d are the a and c wurtzite lattice parameters of the matrix and QD, respectively. The effective dots/matrix mismatch can then be defined as

$$\varepsilon^* = f = \frac{2f_a + f_c}{3}. \tag{39}$$
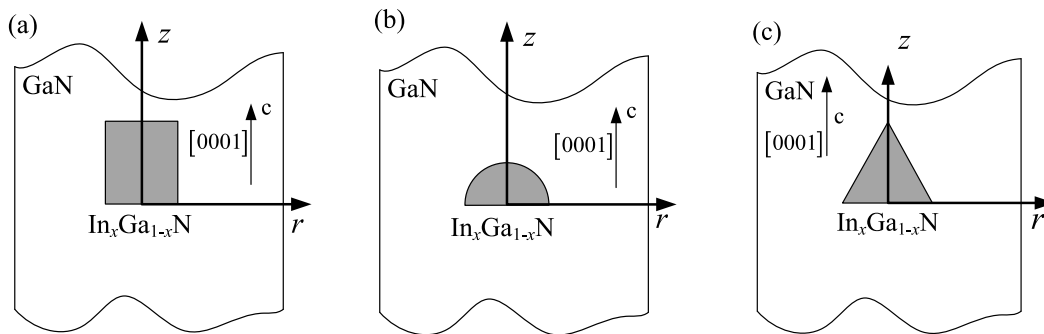
Fig. 8. Schematic depiction of In$_x$Ga$_{1-x}$N QDs or Al$_y$Ga$_{1-y}$N QDs in shape of cylinder (a), truncated sphere (b), and cone (c) in GaN nanowire. Nanowire's axis is oriented along [0001] crystallographic direction (*c*-axis).

Table 4. Effective lattice misfit parameter f for wurtzite III-nitrides.

Material		Misfit parameter f
Quantum dots	Matrix	
GaN	AlN	0.029
$In_{0.2}Ga_{0.8}N$	GaN	0.021
$In_{0.5}Ga_{0.5}N$	GaN	0.050
$Al_{0.2}Ga_{0.8}N$	GaN	−0.006
$Al_{0.5}Ga_{0.5}N$	GaN	−0.015

Table 5. Crystal lattice parameters (given in Å) of $In_xGa_{1-x}N$ and $Al_yGa_{1-y}N$ with wurtzite structure (at 300 K).

Lattice parameters	$In_{0.2}Ga_{0.8}N$	$In_{0.5}Ga_{0.5}N$	$Al_{0.2}Ga_{0.8}N$	$Al_{0.5}Ga_{0.5}N$
a	3.258	3.361	3.174	3.151
c	5.287	5.440	5.145	5.084

The values of effective lattice misfit parameter f of $In_xGa_{1-x}N$ and $Al_yGa_{1-y}N$ dots in GaN matrix are shown in Table 4.

For the crystal lattice parameters a and c of wurtzite structures $In_xGa_{1-x}N$, $Al_yGa_{1-y}N$, Vegard's law is applied [53,54]:

$$a_{In_xGa_{1-x}N} = x \cdot a_{InN} + (1-x) \cdot a_{GaN}, \quad (40a)$$

$$c_{In_xGa_{1-x}N} = x \cdot c_{InN} + (1-x) \cdot c_{GaN}, \quad (40b)$$

$$a_{Al_yGa_{1-y}N} = y \cdot a_{AlN} + (1-y) \cdot a_{GaN}, \quad (40c)$$

$$c_{Al_yGa_{1-y}N} = y \cdot c_{AlN} + (1-y) \cdot c_{GaN}. \quad (40d)$$

With the support of Eqs. (40), we can calculate the lattice constants of $In_xGa_{1-x}N$ and $Al_yGa_{1-y}N$. The results are shown in the Table 5.

The expressions of the elastic field of QDs in the nanowire (as mentioned in Section 2) are applied to an isotropic elastic medium. However, wurtzite GaN is elastically anisotropic. Therefore, we use the effective Poisson's ratio according to the expression, which was derived by averaging Poisson's ratios along the three mutually perpendicular axes chosen in characteristic crystallographic directions, as in Ref. [29]:

$$\overline{\nu} = -\frac{1}{3}\left(\frac{s_{13}}{s_{33}} + \frac{s_{12} + s_{13}}{s_{11}}\right), \quad (41)$$

where s_{ij} are the elastic compliances for GaN. Using the elastic constants from Ref. [55] we obtain $\overline{\nu} = 0.234$.

6. THE INFLUENCE OF SURFACE EFFECTS ON THE BAND STRUCTURE

The change of the VB structure is *nonlinear* with strain as these energies represent the eigenvalues of a 6×6 Hamiltonian in the **k·p** calculations (see Section 3 for details). We will examine the shifts of the CB and VB edges due to QD strain field by utilizing the **k·p** perturbation approach developed by Bir and Pikus [10] and employing the corresponding deformation potentials for GaN [47].

Under the influence of strain, both CB and VB are strongly shifted. The positions of heavy-hole (HH), light-hole (LH), and crystal-field split-off hole (CH) change compared to their equilibrium positions and can even cross each other. Therefore, to simplify we label the individual VBs as top, middle, and bottom VB according to their energy, with the top VB being closest to the CB bottom.

The dependence of CB on strain is determined by Eq. (33). We see that CB bottom depends linearly on hydrostatic strain. This means that it depends on the free surface conditions and the interaction of the free surface with the quantum dots buried under it. The dependence of the VBs on strains (see Eqs. (31)) is more complex than that of CB.

Fig. 9 shows edge of CB shift due to strain for $In_{0.2}Ga_{0.8}N$ and $Al_{0.2}Ga_{0.8}N$ dots. The results clearly reveal two opposite trends. For $In_{0.2}Ga_{0.8}N$ dots in GaN matrix, outside the dot, CB edge decreases by hundreds of meV. Calculations indicate that the most significant reduction in the band gap occurs at the nanowire surface, specifically at the intersection of the plane perpendicular to the nanowire axis that divides the dot into two equal-volume parts (see Figs. 9a–c). Similarly, for $Al_{0.2}Ga_{0.8}N$ dots in GaN matrix, the edge of CB outside the dot increases by tens of meV. This increase is also most pronounced at the nanowire surface, at the intersection of the plane perpendicular to the nanowire axis that divides the dot into two equal-volume regions (see Figs. 9d–f).

For points outside the dots, near the nanowire axis, the band gap tends to decrease for both $In_{0.2}Ga_{0.8}N$ and $Al_{0.2}Ga_{0.8}N$ dots. However, along the wire surface, the band gap decreases for the $In_{0.2}Ga_{0.8}N$ dot. For the $Al_{0.2}Ga_{0.8}N$ dot, the behavior is more complex, with a slight increase in band gap. The change of the band gap depends on the shape of QDs; see Fig. 10.

7. STRESSOR-INDUCED POLARIZATION CHARGES

The fixed polarized charge density in the system is related to the variation of total polarization **P** with position. Total polarization **P** includes spontaneous polarization **P**sp and piezoelectric polarization **P**pz. The piezoelectric polarization vector **P**pz at an arbitrary point is determined according to Eq. (34). The fixed polarized charge density is determined by the expression: $\rho(x,y,z) = -\nabla\mathbf{P}$. The fixed polarized charge density approaches the range $10^{10} |e|/cm^3$ when approaching the surface of QDs; see
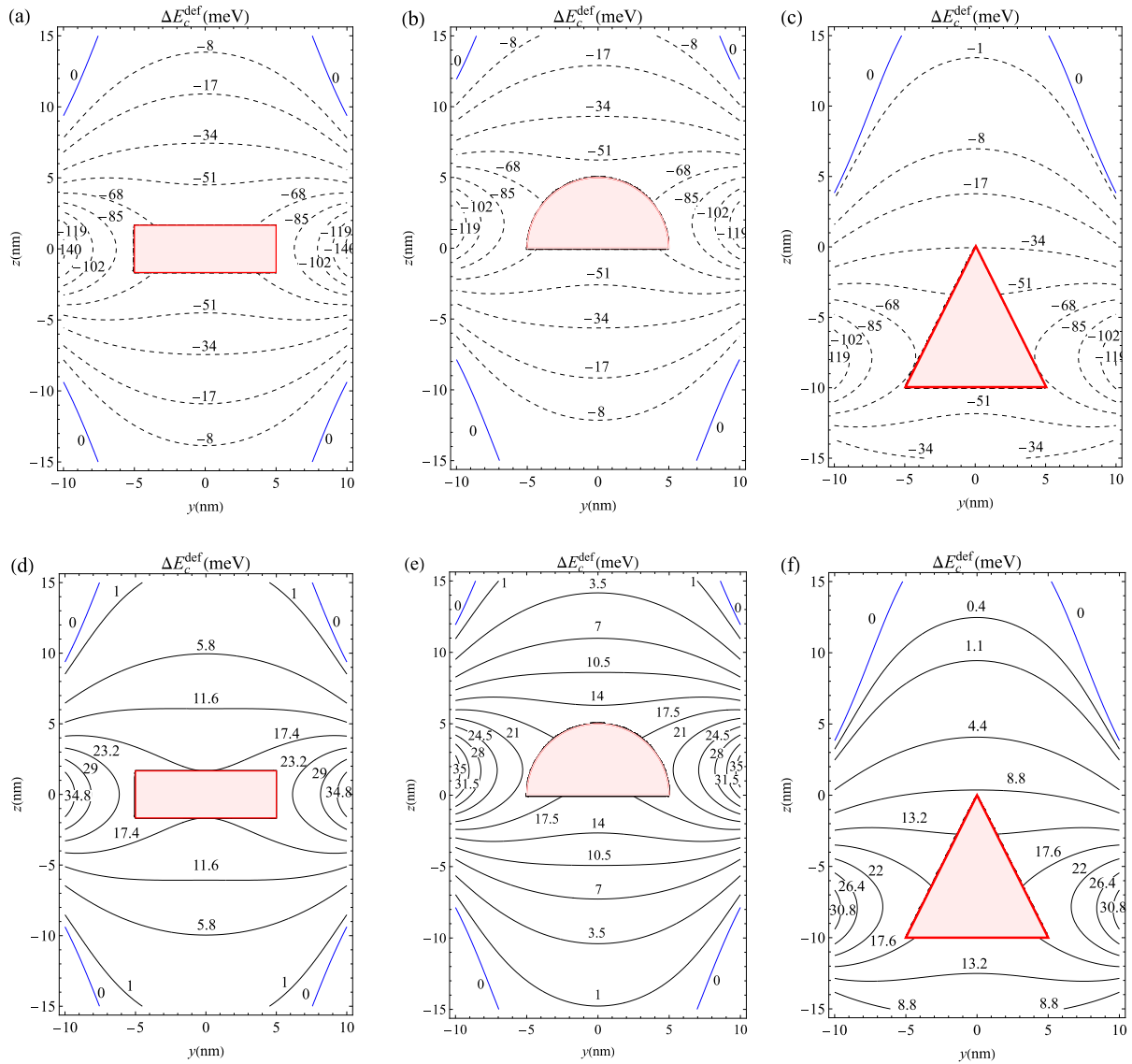
Fig. 9. The contour maps for GaN CB edge changes ΔE_c^{def} (given in meV) due to strain fields of CyI in the nanowire: (a) $In_{0.2}Ga_{0.8}N$ dot in GaN wire, and (d) $Al_{0.2}Ga_{0.8}N$ dot in GaN wire; hemispherical quantum dots in the nanowire: (b) $In_{0.2}Ga_{0.8}N$ dot in GaN wire and (e) $Al_{0.2}Ga_{0.8}N$ dot in GaN wire; CI in the nanowire: (c) $In_{0.2}Ga_{0.8}N$ dot in GaN wire and (f) $Al_{0.2}Ga_{0.8}N$ dot in GaN wire. Parameters for calculation: radius of nanowire $a = 10$ nm; the volume of dots is $250\pi / 3$ nm³; the base radius of the dots is $c = 5$ nm; average Poisson's ratio of GaN wurtzite $\overline{\nu} = 0.234$; the misfit parameter of $In_{0.2}Ga_{0.8}N$ and $Al_{0.2}Ga_{0.8}N$ dots in GaN are $\varepsilon^* = 0.021$ and -0.0058, respectively.

Fig. 10. This value is quite small compared to the electron density of GaN which is approximately $2.3 \cdot 10^{18}$ cm⁻³ (at 300 K); see Ref. [52]. This value is also much smaller than the case of ellipsoidal inclusion and point stressor in half-space; see Ref. [29].

The contour plot of the induced charge caused by the strain of QD in the form of a finite cylinder, hemisphere, and cone in the nanowire is shown in Fig. 11.

8. DISCUSSION

Figs. 4–6, and 12 demonstrate that the influence of the surface on the hydrostatic strain just beneath it depends on the shape of QD. This effect is strongest for CyI, followed by

the SI, and weakest for CI (see Fig. 12). Indeed, for CyI, the disk radius remains constant, and the ratio between the dot radius c and the nanowire radius a, denoted as $t = c/a$, is constant. In contrast, for SI dot and CI dot, the radius c varies along the symmetry axis, so the ratio $t = c/a$ also changes along this direction and is always smaller than in the cylindrical case. As a result, the surface effect on the hydrostatic strain inside the nanowire is strongly dependent on the shape of the embedded dot. Consequently, the edge of CB is also shape-dependent, as shown in Figs. 9 and 13.

The presence of strain induced by the embedded dot simultaneously affects both CB (see Eq. (33)) and VB (see Eq. (31)) of the material. As a result, the band gap of the
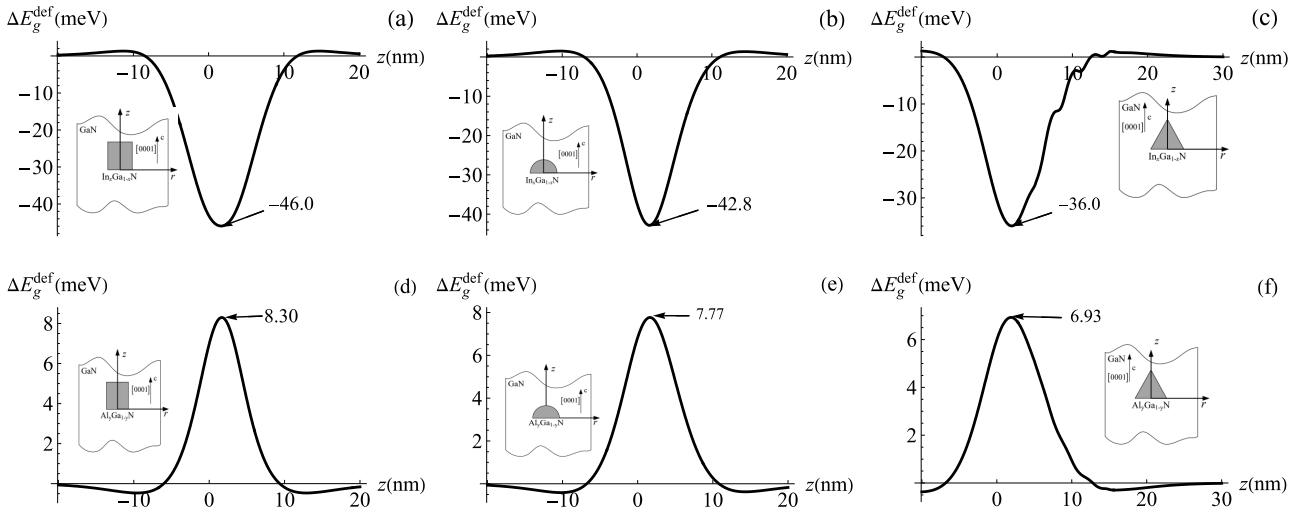
Fig. 10. The change of the band gap ΔE_g^{def} of GaN along free surface of the wire due to the presence of the In$_{0.2}$Ga$_{0.8}$N (a–c) and Al$_{0.2}$Ga$_{0.8}$N (d–f) QDs. Parameters for calculation: radius of nanowire $a = 10$ nm; the selected quantum dots have a volume of $250\pi/3$ nm^3; the radius of the base $c = 5$ nm; average Poisson's ratio of GaN wurtzite $\overline{v} = 0.234$; the misfit parameter of In$_{0.2}$Ga$_{0.8}$N and Al$_{0.2}$Ga$_{0.8}$N dots in GaN are $\varepsilon^* = 0.021$ and -0.0058, respectively.

Fig. 11. Contour maps for the fixed polarization charge density are given in unit of $10^{10}\,|e|/cm^3$ for In$_{0.2}$Ga$_{0.8}$N QDs in GaN nanowire: (a) cylinder, (b) hemisphere, (c) cone with the same volume and base radius. The parameters for calculation: volume and radius of base of QDs are $250\pi/3$ nm^3 and 5 nm, respectively; radius of the wire is 10 nm; Poisson's ratio $\overline{v} = 0.234$; misfit parameter of In$_{0.2}$Ga$_{0.8}$N dot in GaN matrix is $\varepsilon^* = 0.021$; the piezoelectric coefficients for GaN are given in Table 1.
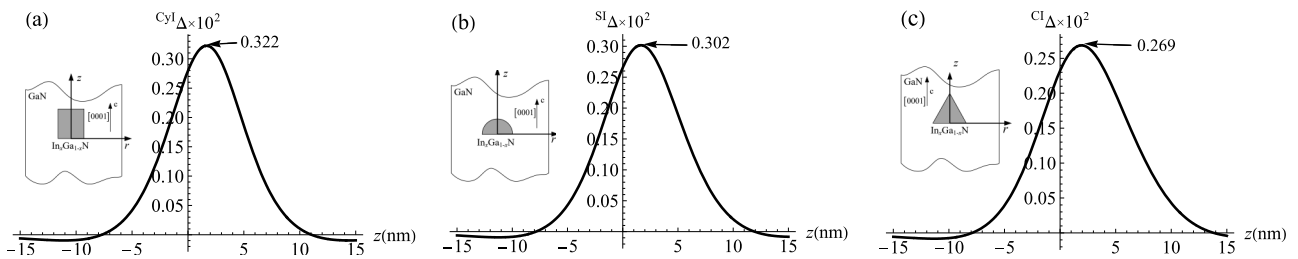
Fig. 12. The distribution of hydrostatic strain along the surface of the wire caused by In$_{0.2}$Ga$_{0.8}$N dots embedded in the GaN nanowire: (a) cylindrical QD, (b) hemispherical QD, (c) conical QD. The parameters for calculations: the volume and the radius of base of QD are $250\pi/3$ nm^3 and 5 nm, respectively; the radius of the nanowire is 10 nm; average Poisson's ratio $\overline{v} = 0.234$ for GaN; the misfit parameter of In$_{0.2}$Ga$_{0.8}$N dot in matrix GaN is $\varepsilon^* = 0.021$.
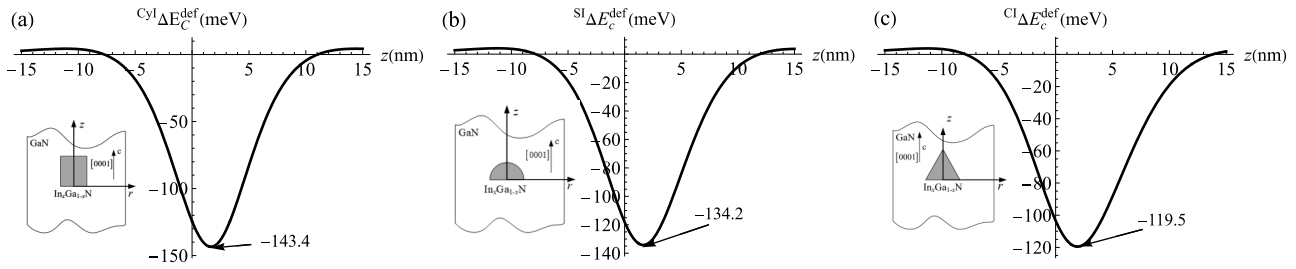
Fig. 13. The change of CB edge along the surface of the wire caused by $In_{0.2}Ga_{0.8}N$ dots embedded in the GaN nanowire: (a) cylindrical QD, (b) hemispherical QD, (c) conical QD. The parameters for calculations: volume and radius of base of QD are $250\pi/3$ nm^3 and 5 nm, respectively; radius of the nanowire is 10 nm; average Poisson's ratio is $\overline{v} = 0.234$ for GaN; misfit parameter of $In_{0.2}Ga_{0.8}N$ dot in GaN matrix is $\varepsilon^* = 0.021$.
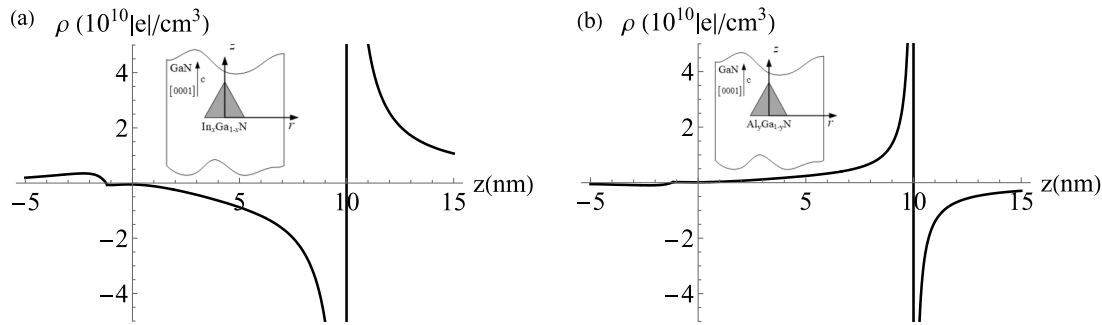
Fig. 14. The distribution of induced fixed polarization charge density along the symmetry axis ($r = 0$) of the conical QD is given in units of 10^{10} |e|/cm^3 for $In_{0.2}Ga_{0.8}N$ dot (a) and $Al_{0.2}Ga_{0.8}N$ dot (b) in GaN nanowire. The parameters for calculations: radius and height of the cone are $c = 5$ nm and $h = 10$ nm, respectively; Poisson's ratio $\overline{v} = 0.234$; misfit parameters are $\varepsilon^* = 0.021$, -0.0058 for $In_{0.2}Ga_{0.8}N$ and $Al_{0.2}Ga_{0.8}N$ dots in GaN matrix, respectively; the piezoelectric coefficient for GaN are given in Table 1.

material is altered in the presence of the dot. Figs. 10a–c show the influence of the surface on the band gap just beneath the nanowire surface. Here, the variation in the band gap directly beneath the surface clearly depends on the shape of the dot, namely: $\Delta E_g^{def} \approx -46.0$, -42.8, and -36.0 meV for CyI, SI, and CI, respectively; corresponding to a reduction in band gap width of 1.32%, 1.23%, and 1.03% compared to unstrained GaN. The variation in band gap is directly related to the energy of strain of the dots. Furthermore, the study shows that the elastic energy of the dot embedded in the wire depends on the ratio $t = c/a$ (see Ref. [32]). Here, it is evident that for cylindrical dots, $t = c/a$ remains constant, while for SI and CI, the value of ratio t varies along the symmetry axis z. As previously mentioned, the band gap beneath the wire surface decreases most significantly for CyI.

The presence of QDs in the wire gives rise to fixed polarized charges in the dots and in the wire. However, the density of fixed polarized charges is quite small (about 10^{10} |e|/cm^3); see Figs. 11 and 14. This charge density can be easily screened by free electrons, considering the usually reported unintentional n-type doping level of $10^{16} \div 10^{17}$ |e|/cm^3 in GaN. For points near the top of the conical QD, the fixed polarization charge density increases abruptly: for $In_{0.2}Ga_{0.8}N$ conical QD in GaN matrix, see

Fig. 14a and for $Al_{0.2}Ga_{0.8}N$ conical QD in GaN matrix, see Fig. 14b.

9. CONCLUSIONS

In this study we investigated the influence of strain of QDs in nanowire on electronic band structures of III-nitride. QDs chosen are ternary semiconductor compounds of III-nitride $In_xGa_{1-x}N$, $Al_yGa_{1-y}N$ with $x,y = 0.2$ in wurtzite structure. We assume that the matrix is isotopically homogeneous with an average Poisson's ratio $\overline{v} = 0.234$.

The influence of the nanowire surface on the band gap clearly depends on the shape of the dots. This effect is related to the ratio between the dot's and nanowire's radii. For $In_{0.2}Ga_{0.8}N$ QDs with identical volumes and a base radius of 5 nm embedded in a GaN nanowire of 10 nm radius, the band gap just beneath the surface shows the most significant reduction for the cylindrical dot—up to 1.32% lower compared to the band gap of unstrained GaN (at 300 K). The reduction in band gap is related to the elastic energy of QDs embedded in the nanowire.

In addition, the presence of strain generated by QDs in the nanowire also causes the fixed polarized charge of the III-nitride structure around the dots to appear. How-

ever, fixed polarized charge density is small compared to the free electron density in *n*-GaN. This fixed polarized charge density can be easily screened by free electrons in *n*-GaN.

ACKNOWLEDGEMENTS

REFERENCES

[1] R.A. Ferreyra, C. Zhu, A. Teke, H. Morkoç, Group III Ni-trides, in: S. Kasap, P. Capper (Eds.), Springer Handbook of Electronic and Photonic Materials, Springer, Cham, 2017.

[2] J.I. Pankove, E.A. Miller, J.E. Berkeyheiser, GaN blue light-emitting diodes, *Journal of Luminescence*, 1972, vol. 5, no. 1, pp. 84–86.

[3] M.S. Shur, GaN based transistors for high power applications, *Solid-State Electronics*, 1998, vol. 42, no. 12, pp. 2131–2138.

[4] C. Zhao, Y.H. Chen, B. Xu, C.G. Tang, Z.G. Wang, F. Ding, Study of the wetting layer of InAs/GaAs nanorings grown by droplet epitaxy, *Applied Physics Letters*, 2008, vol. 92, no. 6, art. no. 063122.

[5] J. Yan, J. Wang, P. Cong, L. Sun, N. Liu, Z. Liu, C. Zhao, J. Li, Improved performance of UV-LED by p-AlGaN with graded composition, *Physica Status Solidi C*, 2011, vol. 8, no. 2, pp. 461–463.

[6] J. Yan, J. Wang, Y. Zhang, P. Cong, L. Sun, Y. Tian, C. Zhao, J. Li, AlGaN-based deep-ultraviolet light-emitting diodes grown on high-quality AlN template using MOVPE, *Journal of Crystal Growth*, 2015, vol. 414, pp. 254–257.

[7] F. Bernardini, V. Fiorentini, D. Vanderbilt, Spontaneous polarization and piezoelectric constants of III-V nitrides, *Physical Review B*, 1997, vol. 56, no. 16, pp. R10024–R10027.

[8] F. Bernardini, V. Fiorentini, Spontaneous versus Piezo-electric Polarization in III-V Nitrides: Conceptual Aspects and Practical Consequences, *Physica Status Solidi B*, 1999, vol. 216, no. 1, pp. 391–398.

[9] F. Bernardini, V. Fiorentini, Nonlinear macroscopic polarization in III-V nitride alloys, *Physical Review B*, 2001, vol. 64, no. 8, art. no. 085207.

[10] G.L. Bir, G.E. Pikus, P. Shelnitz, D. Louvish, *Symmetry and strain-induced effects in semiconductors*, Wiley, New York, 1974.

[11] C.P. Kuo, S.K. Vong, R.M. Cohen, G.B. Stringfellow, Effect of mismatch strain on band gap in III-V semiconductors, *Journal of Applied Physics*, 1985, vol. 57, no. 12, pp. 5428–5432.

[12] T. Manku, A. Nathan, Valence energy-band structure for strained group-IV semiconductors, *Journal of Applied Physics*, 1993, vol. 73, no. 3, pp. 1205–1213.

[13] M.V. Fischetti, S.E. Laux, Band structure, deformation potentials, and carrier mobility in strained Si, Ge, and SiGe alloys, *Journal of Applied Physics*, 1996, vol. 80, no. 4, pp. 2234–2252.

[14] Y. Sun, S.E. Thompson, T. Nishida, *Strain Effect in Semiconductors*, Springer, New York, NY, 2010.

[15] M. Hetzl, M. Kraut, J. Winnerl, L. Francaviglia, M. Döblinger, S. Matich, A. Fontcuberta i Morral, M. Stutzmann, Strain-Induced Band Gap Engineering in Selectively Grown GaN–(Al,Ga)N Core–Shell Nanowire Heterostructures, *Nano Letters*, 2016, vol. 16, no. 11, pp. 7098–7106.

[16] M. Benaissa, W. Sigle, H. Zaari, M. Tadout, P.A. van Aken, Strain and size combined effects on the GaN band structure: VEELS and DFT study, *Physical Chemistry Chemical Physics*, 2017, vol. 19, no. 7, pp. 5430–5434.

[17] M. Sopanen, H. Lipsanen, J. Tulkki, J. Ahopelto, Strain-induced quantum dot superlattice, *Physica E: Low-dimensional Systems and Nanostructures*, 1998, vol. 2, no. 1–4, pp. 19–22.

[18] A.E. Romanov, G.E. Beltz, W.T. Fischer, P.M. Petroff, J.S. Speck, Elastic fields of quantum dots in subsurface layers, *Journal of Applied Physics*, 2001, vol. 89, no. 8, pp. 4523–4531.

[19] E. Melezhik, O. Korotchenkov, Elastic fields of quantum dots in semi-infinite matrices: Green's function analytical analysis, *Journal of Applied Physics*, 2009, vol. 105, no. 2, art. no. 023505.

[20] N.A. Bert, A.L. Kolesnikova, I.K. Korolev, A.E. Romanov, A.B. Freidin, V.V. Chaldyshev, E.C. Aifantis, Elastic fields and physical properties of surface quantum dots, *Physics of the Solid State*, 2011, vol. 53, no. 10, pp. 2091–2102.

[21] T. Mura, *Micromechanics of defects in solids*, Springer, Dordrecht, 1987.

[22] J.D. Eshelby, The determination of the elastic field of an ellipsoidal inclusion, and related problems, *Proceedings of the Royal Society A: Mathematical, Physical and Engineering Sciences*, 1957, vol. 241, no. 1226, pp. 376–396.

[23] J.D. Eshelby, The elastic field outside an ellipsoidal inclusion, *Proceedings of the Royal Society A: Mathematical, Physical and Engineering Sciences*, 1959, vol. 252, no. 1271, pp. 561–569.

[24] A.L. Kolesnikova, M.Yu. Gutkin, A.E. Romanov, Elastic models of defects in 3D and 2D crystals, *Reviews on Advanced Materials Science*, 2017, vol. 51, pp. 130–148.

[25] A.L. Kolesnikova, M.Yu. Gutkin, A.E. Romanov, Analytical elastic models of finite cylindrical and truncated spherical inclusions, *International Journal of Solids and Structures*, 2018, vol. 143, pp. 59–72.

[26] D. Leonard, K. Pond, P.M. Petroff, Critical layer thickness for self-assembled InAs islands on GaAs, *Physical Review B*, 1994, vol. 50, no. 16, pp. 11687–11692.

[27] R.J. Warburton, Self-assembled semiconductor quantum dots, *Contemporary Physics*, 2002, vol. 43, no. 5, pp. 351–364.

[28] P. Waltereit, A.E. Romanov, J.S. Speck, Electronic properties of GaN induced by a subsurface stressor, *Applied Physics Letters*, 2002, vol. 81, no. 25, pp. 4754–4756.

[29] A.E. Romanov, P. Waltereit, J.S. Speck, Buried stressors in nitride semiconductors: Influence on electronic properties, *Journal of Applied Physics*, 2005, vol. 97, no. 4, art. no. 043708.

[30] A.E. Romanov, A.L. Kolesnikova, M.Yu. Gutkin, V.G. Dubrovskii, Elasticity of axial nanowire heterostructures with sharp and diffuse interfaces, *Scripta Materialia*, 2020, vol. 176, pp. 42–46.

[31] A.L. Kolesnikova, R.M. Soroka, A.E. Romanov, Defects in the elastic continuum: classification, fields and phys-

ical analogies, *Materials Physics and Mechanics*, 2013, vol. 17, no. 1, pp. 71–91.

[32] A.L. Kolesnikova, N. Van Tuyen, M.Yu. Gutkin, A.E. Romanov, Dilatational disk and finite cylindrical inclusion in elastic nanowire, *International Journal of Engineering Science*, 2025, vol. 206, art. no. 104169.

[33] G. Eason, B. Noble, I.N. Sneddon, On certain integrals of Lipschitz-Hankel type involving products of Bessel functions, *Philosophical Transactions of the Royal Society of London. Series A, Mathematical and Physical Sciences*, 1955, vol. 247, no. 935, pp. 529–551.

[34] A.L. Kolesnikova, N. Van Tuyen, M.Yu. Gutkin, A.E. Romanov, General approach to calculating elastic characteristics of axisymmetric quantum dots in whisker-like nanocrystals, *Technical Physics Letters*, 2024, vol. 50, no. 6, pp. 28–32 (in Russian).

[35] G.B. Dwight, *Tables of integrals and other mathematical formulas*, Fourth edition, The Macmillan Company, New York, 1961.

[36] K. Pearson, *Tables of Incomplete Beta-Function*, 2nd ed., Cambridge University Press, Cambridge, 1968.

[37] V.T. Nguyen, A.L. Kolesnikova, A.E. Romanov, Isotropic elasticity of dilatational conical inclusion. An analytical approach, *International Journal of Solids and Structures*, 2024, vol. 294, art. no. 112735.

[38] B.M. Dwork, *Generalized Hypergeometric Functions*, 1st edition, Clarendon Press, 1990.

[39] M.H. Sadd, *Elasticity: Theory, Applications, and Numerics*, Elsevier Butterworth–Heinemann, 2005.

[40] H. Zhu, S. Feng, D. Jiang, Y. Deng, H. Wang, Strain Effect on the Band Structure of InAs/GaAs Quantum Dots, *Japanese Journal of Applied Physics*, 1999, vol. 38, no. 11R, art. no. 6264.

[41] A.E. Romanov, T.J. Baker, S. Nakamura, J.S. Speck, Strain-induced polarization in wurtzite III-nitride semipolar layers, *Journal of Applied Physics*, 2006, vol. 100, no. 2, art. no. 023522.

[42] A. Zhang, S. Luo, G. Ouyang, G. Yang, Strain-induced optical absorption properties of semiconductor nanocrystals, *Journal of Chemical Physics*, 2013, vol. 138, no. 24, art. no. 244702.

[43] J.M. Luttinger, W. Kohn, Motion of Electrons and Holes in Perturbed Periodic Fields, *Physical Review Journals Archive*, 1955, vol. 97, no. 4, pp. 869–883.

[44] S.L. Chuang, *Physics of Optoelectronic Devices*, John Wiley, New York, USA, 1995.

[45] S.L. Chuang, C.S. Chang, k·p method for strained wurtzite semiconductors, *Physical Review B*, 1996, vol. 54, no. 4, pp. 2491–2504.

[46] M. Willatzen, L.C. Lew Yan Voon, *The kp Method*, Springer Berlin, Heidelberg, 2009.

[47] S. Ghosh, P. Waltereit, O. Brandt, H.T. Grahn, K.H. Ploog, Electronic band structure of wurtzite GaN under biaxial strain in the M plane investigated with photoreflectance spectroscopy, *Physical Review B*, 2002, vol. 65, no. 7, art. no. 075202.

[48] C. Wood, D. Jena (Eds.), *Polarization Effects in Semiconductors*, Springer New York, NY, 2008.

[49] J.F. Nye, *Physical Properties of Crystals: Their Representation by Tensors and Matrices*, Oxford University Press, USA, 1985.

[50] M.T. Hibberd, V. Frey, B.F. Spencer, P.W. Mitchell, P. Dawson, M.J. Kappers, R.A. Oliver, C.J. Humphreys, D.M. Graham, Dielectric response of wurtzite gallium nitride in the terahertz frequency range, *Solid State Communications*, 2016, vol. 247, pp. 68–71.

[51] J.G. Gualtieri, J.A. Kosinski, A. Ballato, Piezoelectric materials for acoustic wave applications, *IEEE Transactions on Ultrasonics, Ferroelectrics, and Frequency Control*, 1994, vol. 41, no. 1, pp. 53–59.

[52] M.E. Levinshtein, S.L. Rumyantsev, M.S. Shur, Properties of advanced semiconductor materials GaN, AlN, InN, BN, SiC, SiGe, John Wiley & Sons, 2001.

[53] A.R. Denton, N.W. Ashcroft, Vegard's law, *Physical Review A*, 1991, vol. 43, no. 6, pp. 3161–3164.

[54] L. Vegard, Die Konstitution der Mischkristalle und die Raumfüllung der Atome, *Zeitschrift für Physik*, 1921, vol. 5, no. 1, pp. 17–26.

[55] K. Kim, W.R.L. Lambrecht, B. Segall, Elastic constants and related properties of tetrahedrally bonded BN, AlN, GaN, and InN, *Physical Review B*, 1996, vol. 53, no. 24, pp. 16310–16326.

[56] A.L. Kolesnikova, A.E. Romanov, Representations of elastic fields of circular dislocation and disclination loops in terms of spherical harmonics and their application to various problems of the theory of defects, *International Journal of Solids and Structures*, 2010, vol. 47, no. 1, pp. 58–70.

Влияние упругого поля квантовых точек на электронную зонную структуру III-нитридных проволочных полупроводников

Nguyen Van Tuyen [1,2], А.Л. Колесникова [1,3], А.Е. Романов [1]

[1] Университет ИТМО, Кронверкский 49, Санкт-Петербург, 197101, Россия
[2] Sao Do University, No 24, Thai Hoc 2, Sao Do Ward, Chi Linh City, Hai Duong, Vietnam
[3] Институт проблем машиноведения РАН, Большой пр. 61, В.О., Санкт-Петербург, 199178, Россия

Аннотация. В данной работе мы исследуем влияние деформаций, наведённых аксиально-симметричными квантовыми точками цилиндрической, полусферической и конической форм в полупроводниковой III-нитридной нанопроволоке, на зонную структуру материала нанопроволоки. Для изучения упругих свойств квантовых точек использовалась модель упругого включения с собственной деформацией. Для учета влияния свободной поверхности проволоки на упругие поля квантовых точек были получены аналитические решения соответствующих граничных задач. Метод возмущений **k·p** применялся для оценки роли наведённых деформаций в изменении зонной структуры материала. Показано, что изменение ширины запрещенной зоны явно зависит от формы внедренной квантовой точки. Было исследовано влияние наведённых квантовыми точками деформаций на электрополяризацию материала, обладающего пьезоэлектрическими свойствами. Обнаружено, что наибольший скачок плотности электрического заряда достигается вблизи вершины конического включения.

Ключевые слова: III-нитридные полупроводниковые нанопроволоки; квантовые точки; упругие поля; запрещенная зона; электрополяризация